QUALITY ASSESSMENT OF SYNTHETIC APERTURE SONAR IMAGES

Christian Debes[1], *Robert Engel*[2],*Abdelhak M. Zoubir*[1] *and Arne Kraft*[2]

[1]Signal Processing Group
Technische Universität Darmstadt
Darmstadt, Germany

[2]ATLAS ELEKTRONIK GmbH
Applied Research
Bremen, Germany

ABSTRACT

We consider the problem of navigation error detection in synthetic aperture sonar images. Specifically, the effect of errors in the position and attitude of the sonar antenna is explored in the image and frequency domain. We present two metrics which can be used to discriminate between images with different degrees of navigation errors. A systematic test is developed which allows an automatic detection of navigation errors. Simulated synthetic aperture sonar images are used to test the presented methods.

1. INTRODUCTION

The principle of synthetic aperture sonar (SAS) [3] is to create virtual antenna structures when combining the signals generated by multiple pings from a single physical antenna in motion. Ideally, the pose trajectory of the physical antenna is represented by a straight line for the reference position and a constant attitude for the antenna to form a perfect linear virtual array. However, deviations from this ideal trajectory are unavoidable due to external physical disturbances acting on the sensor carrier. If the stave positions (i.e. the pose trajectory of the antenna) are known precisely, they can be taken into account within the SAS image reconstruction algorithm. Hence a precise knowledge of the sensor position at each point in time is crucial for a successful SAS image reconstruction.

In practice, the sensor position estimates are subject to errors of the navigation system of the sensor carrier. Unfortunately, this estimation imperfection can lead to serious degradations of the SAS performance. As a consequence, the sensitivity of the SAS performance against pose estimation errors is crucial for a common design of an SAS system and the underlying navigation system.

Navigation errors which vary over the synthetic antenna length lead to an out-of-focus effect, i.e. an increasing local image variability around the target which complicates, e.g., discrimination of two closely spaced targets or estimation of the true target contours.

In this paper, we consider the problem of assessment of navigation accuracy which is relevant to an SAS system. We present several metrics which only use the information at hand, i.e. the SAS image itself. This is of high practical interest and will enable a systematic decision as to the quality of an SAS image in view of navigation errors. Based on different metrics, hypothesis tests are used to automatically distinguish between SAS images with and without navigation errors. The performance of the proposed metrics is assessed based on simulated SAS images. Based on these results, we confirm the practicability of the proposed techniques in view of accuracy and implementability.

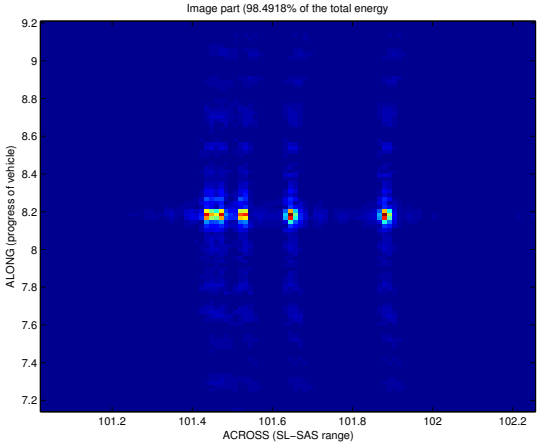

(a) Close-up: SAS image without navigation errors

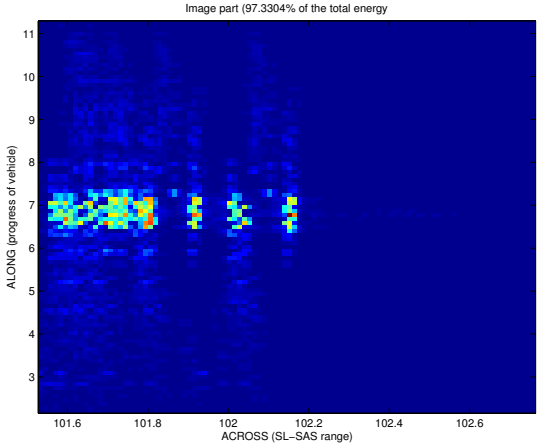

(b) Close-up: SAS image with navigation errors

Fig. 1. SAS images including five point scatterers

2. DATA ANALYSIS

It is our objective to identify features in SAS images that can be used to discriminate among scenarios with and without navigation errors. These features shall then be used to derive

procedures that perform automatic detection of navigation errors. For all data sets the scene is represented by a line of five point scatterers. Five images were generated for different orientations of this scene (horizontal, oblique and vertical). A high fidelity sonar simulation tool [1] was used to generate the image data, the target range is approximately 100 m. The perturbed navigation data have been created with sensor level error models for a typical sensor suite of an autonomous underwater vehicle, comprising models for an inertial measurement unit, a depth sensor and a Doppler velocity log.
Two typical close-ups of these SAS images, one with and one without navigation errors are shown in Figure 1 (a) and (b). As can be seen, the presence of navigation errors leads to an out-of-focus effect which complicates target detection and discrimination. This increased local image variability will be used in the following as a measure to detect navigation errors.

3. PROPOSED METHODS

We present selected methods, developed to tackle the problem of navigation error detection in SAS images. The metrics used to discriminate among SAS images with and without navigation errors are classified as follows:

- **Probabilistic metric:** Here, we consider metrics which operate directly on the data in the image domain. Navigation errors can be detected based on probability density functions (pdf's). The proposed method is based on the Hill estimator [5].
- **Spectral domain-based metric:** The presence of navigation errors leads to differences in the structure of the two-dimensional spectrum, especially when considering the high-frequency region. We present two metrics to detect the structural differences in the spectrum and thus allow for discrimination between SAS images with and without navigation errors.

3.1. Preprocessing

In order to concentrate on the region of interest in SAS images, two preprocessing steps have been taken place before applying the different approaches for evaluating the navigation accuracy. They are:

1. Cropping: The region of interest manifests itself as higher pixel values in the scene. Therefore, we crop the SAS image by taking a window of size 100×100 around the maximum pixel value in the scene. By performing the cropping operation approx. $90 - 99\%$ of the signal energy is preserved while reducing the data size considerably

2. Normalization: The dynamic range of the SAS images differs according to their level of navigation accuracy. Therefore, we normalize the cropped SAS images in order to remove this effect. The normalization is done using:

$$X(n,m) = \frac{X_0(n,m) - \min(X_0(n,m))}{\max(X_0(n,m)) - \min(X_0(n,m))} \quad (1)$$

where $X_0(n,m)$ with $n = 1, ..., N_0$ and $m = 1, ..., M_0$ is the original SAS image and $X(n,m)$ with $n = 1, ..., 100$ and $m = 1, ..., 100$ is the cropped and normalized SAS image which will be used in the sequel. Note that $X(n,m) \in [0,\ 1]\ \forall\ n, m$

3.2. Probabilistic metrics

Initial probabilistic analysis of the SAS images has indicated that they show different probability distributions due to the inherent navigation errors. Typical estimates of the probability density function (pdf) which have been obtained using kernel density estimators [6] can be seen in Figure 2. As can be seen, the presence of navigation errors leads to heavier tails in the density function. To cope with this effect, we use the Hill estimator to quantitatively measure the differences between pdf's.

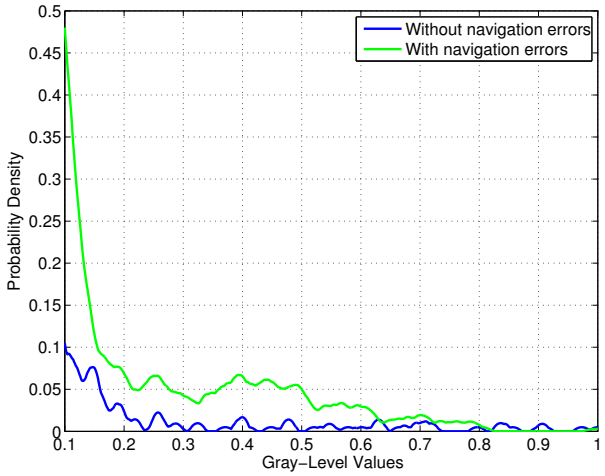

Fig. 2. Kernel density estimation.

The Hill estimator provides an estimate of the tail index $\hat{\alpha}_k$ as:

$$\hat{\alpha}_k = \left\{ \frac{1}{k-1} \sum_{i=1}^{k-1} \ln \frac{X_{(i)}}{X_{(k)}} \right\}^{-1}. \quad (2)$$

where $X_{(i)}$, $i = 1, 2, \ldots, N$ are the descending order statistics from the sequence of observations with X representing the vectorized image and $k > 1$ being the number of tail observations. The estimated tail index for all five scenarios with and without navigation errors are presented in Figure 3 where we empirically chose $k = 45$.
The results of Figure 2 confirm our conjecture that the scenarios with navigation errors tend to be heavy-tailed distributed, yielding a larger tail index.

3.3. Spectral-domain based metrics

An alternative way of detecting navigation errors from SAS images is to search for differences in the two-dimensional spectrum [2]. The structure of the 2D spectrum differs, depending on the strength of navigation errors. We motivate two spectral domain-based metrics to detect the presence of navigation errors. The 2D spectra of the SAS images from

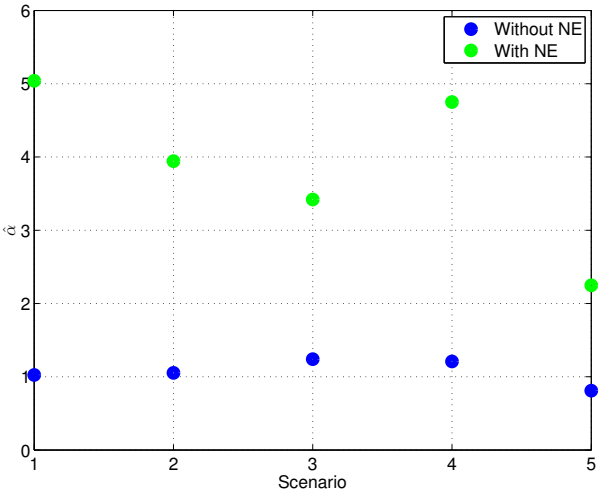

Fig. 3. $\hat{\alpha}$ for all scenarios.

Figures 1 (a) and (b) are shown in Figure 4 (a) and (b). Here, the 2D periodogram has been used as a spectral estimator, i.e.

$$\hat{C}_{XX}(e^{j\omega_1}, e^{j\omega_2}) = \frac{1}{NM}\left|\sum_{n=0}^{N-1}\sum_{m=0}^{M-1} X(n,m)e^{-j(\omega_1 n+\omega_2 m)}\right|^2 \tag{3}$$

An increased signal energy in the high-frequency region can be observed when navigation errors are present. This motivates to use the following metric:

$$\mathcal{E}(\hat{C}_{XX}(e^{j\omega_1}, e^{j\omega_2})) = \sum_{(\omega_1,\omega_2)\in R} \hat{C}_{XX}(e^{j\omega_1}, e^{j\omega_2}) \tag{4}$$

The region R should be chosen in such a way that the high-frequency components of the spectrum is included, e.g. the second spectral quadrant:

$$R = \{(\omega_1, \omega_2) | \omega_1 > \pi/2 \text{ and } \omega_2 > \pi/2\} \tag{5}$$

The results when using the above presented metric can be seen in Figure 5.

As can be seen, the SAS images without and with navigation errors can be well separated using the energy in the second spectral quadrant as a metric.

4. DETECTION OF NAVIGATION ACCURACY

In order to perform a systematic test for navigation errors, a hypothesis test framework [4] is exemplarily derived for the energy metric in a region of the 2D spectrum and the Hill estimator. We consider the two hypotheses

H_0: no navigation errors present
H_1: navigation errors present

4.1. Spectral energy driven systematic tests

The summation over a large number of samples in Equation (4) motivates to model $\mathcal{E}(\hat{C}_{XX}(e^{j\omega_1}, e^{j\omega_2}))$ via the central limit theorem as being Gaussian distributed with mean

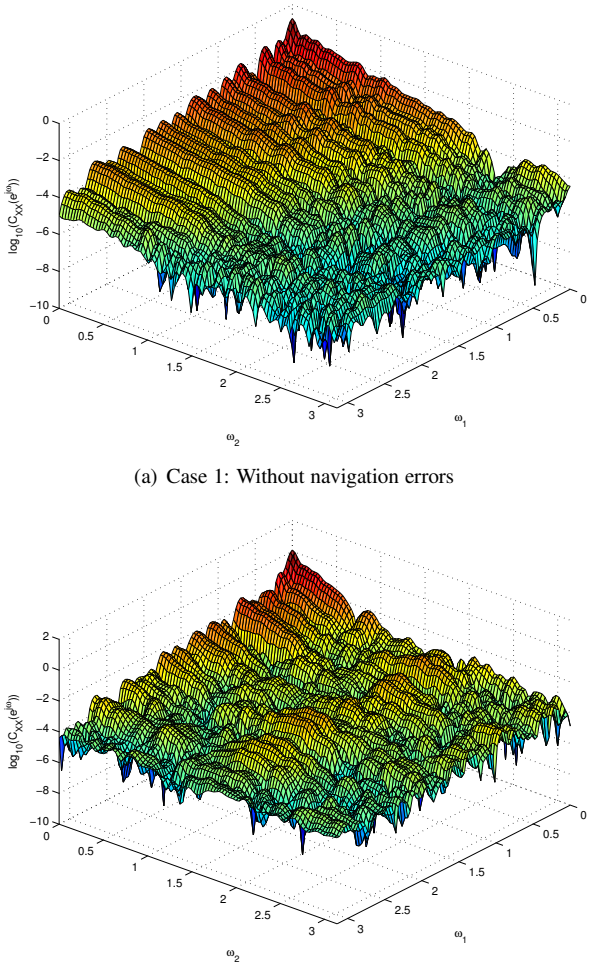

(a) Case 1: Without navigation errors

(b) Case 2: With navigation errors

Fig. 4. 2D-Spectra

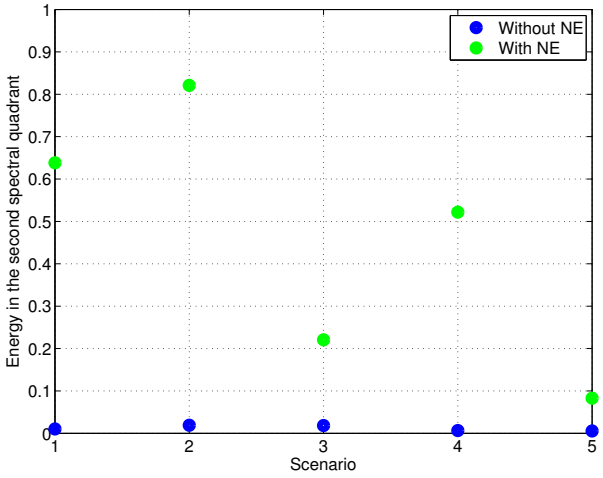

Fig. 5. Energy in the second spectral quadrant

(μ_0, σ_0) and (μ_1, σ_1) for H_0 and H_1 respectively. For the test to be performed we use the conditional probability density

functions

$$p(\mathcal{E}(\hat{C}_{XX}(e^{j\omega_1},e^{j\omega_2}))|H_0) = \frac{1}{\sqrt{2\pi}\sigma_0}\cdot e^{-\frac{(\mathcal{E}(\hat{C}_{XX}(e^{j\omega_1},e^{j\omega_2}))-\mu_0)^2}{2\sigma_0^2}} \quad (6)$$

and

$$p(\mathcal{E}(\hat{C}_{XX}(e^{j\omega_1},e^{j\omega_2}))|H_1) = \frac{1}{\sqrt{2\pi}\sigma_1}\cdot e^{-\frac{(\mathcal{E}(\hat{C}_{XX}(e^{j\omega_1},e^{j\omega_2}))-\mu_1)^2}{2\sigma_1^2}} \quad (7)$$

The likelihood ratio test (LRT) can thus be formulated as

$$\text{LR}(\hat{C}_{XX}(e^{j\omega_1},e^{j\omega_2}))) = \frac{p(\mathcal{E}(\hat{C}_{XX}(e^{j\omega_1},e^{j\omega_2}))|H_1)}{p(\mathcal{E}(\hat{C}_{XX}(e^{j\omega_1},e^{j\omega_2}))|H_0)} \underset{H_0}{\overset{H_1}{\gtrless}} \gamma \quad (8)$$

where γ is the LRT threshold which maximizes the probability of detection, while controlling the probability of false-alarm. For the assumed Gaussian distributions, Equation (8) reduces to

$$\text{LR}(\hat{C}_{XX}(e^{j\omega_1},e^{j\omega_2}))) = \frac{\sigma_0}{\sigma_1}\cdot \exp\left(-\frac{(\mathcal{E}(\hat{C}_{XX}(e^{j\omega_1},e^{j\omega_2}))-\mu_1)^2}{2\sigma_1^2}+\frac{(\mathcal{E}(\hat{C}_{XX}(e^{j\omega_1},e^{j\omega_2}))-\mu_0)^2}{2\sigma_0^2}\right) \underset{H_0}{\overset{H_1}{\gtrless}} \gamma \quad (9)$$

γ can be obtained by fixing a false-alarm rate p_{FA} as

$$p_{FA} = \int_{\gamma}^{\infty} f_L(L|H_0)dL \quad (10)$$

where $f_L(L|H_0)$ is the distribution of the likelihood ratio under the null hypothesis. For the Gaussian distribution assumed above, this reduces to a direct thresholding, i.e.

$$\mathcal{E}(\hat{C}_{XX}(e^{j\omega_1},e^{j\omega_2})) \underset{H_0}{\overset{H_1}{\gtrless}} \beta \quad (11)$$

where β can be found via

$$\beta = \sqrt{2}\sigma_0 \text{erf}^{-1}(1-2p_{FA}) + \mu_0 \quad (12)$$

where erf^{-1} is the inverse error function. In practice, μ_0 and σ_0 are unknown and need to be estimated. This can be done by considering a training data set of SAS images $\left\{X^l(n,m)\right\}_{l=1}^{L}$ under H_0, calculating the metric $\mathcal{E}(\hat{C}^l_{XX}(e^{j\omega_1},e^{j\omega_2}))$ for each data set and then evaluating

$$\hat{\mu}_0 = \frac{1}{L}\sum_{l=1}^{L}\mathcal{E}(\hat{C}^l_{XX}(e^{j\omega_1},e^{j\omega_2})) \quad (13)$$

and

$$\hat{\sigma}_0 = \sqrt{\frac{1}{L-1}\sum_{l=1}^{L}\left(\mathcal{E}(\hat{C}^l_{XX}(e^{j\omega_1},e^{j\omega_2})) - \hat{\mu}_0\right)^2} \quad (14)$$

Applying the presented test using the SAS images presented before we find that the $\mathcal{P}$-Value for the presented test is at 13.2%, i.e. the nominal false-alarm rate p_{FA} can be chosen up to this level without actually causing a false alarm. On the other hand, as long as p_{FA} is chosen to be greater or equal to 1% no missed detection will occur.

4.2. Tail index driven systematic tests

It is known [5] that the Hill estimator is asymptotically normal. This motivates to use a similar test as for the spectral measure, i.e. modelling the null and alternative hypotheses as Gaussian distributions where the parameters of the null hypothesis can be found via a training set of SAS images under H_0. Therefore, we can use the above mentioned test. The parameters μ_0 and σ_0 can be estimated as follows:

$$\hat{\mu}_0 = \frac{1}{L}\sum_{l=1}^{L}\hat{\alpha}_l \quad (15)$$

and

$$\hat{\sigma}_0 = \sqrt{\frac{1}{L-1}\sum_{l=1}^{L}\left(\hat{\alpha}_l - \hat{\mu}_0\right)^2} \quad (16)$$

Given our data examples, the $\mathcal{P}$-Value for the this test is at 15.67%, i.e. the nominal false-alarm rate p_{FA} can be chosen up to this value without causing a false alarm. On the other hand, when p_{FA} is chosen to be greater or equal to 7.6% no missed detection will occur.

5. CONCLUSION

Two metrics, one in the image and one in the frequency domain have been presented that can be used to discriminate between SAS images with different degrees of navigation errors. A systematic test has been derived which can be used to automatically detect the presence of navigation errors. The presented metrics and tests have been evaluated using simulated SAS images and navigation errors.

6. REFERENCES

[1] H. Bracker, E. Krömer, and D. Rathjen. High fidelity real-time sonar simulation. *Undersea Defence Technology*, June 2008. On CD ROM.

[2] J. Cadzow and K. Ogina. Two-dimensional spectral estimation. *IEEE Transactions on Acoustics, Speech, and Signal Processing*, 29:396–401, 1981.

[3] B.L. Douglas and H. Lee. Synthetic aperture active sonar imaging. In *IEEE International Conference on Acoustics, Speech, and Signal Processing*, volume 3, pages 37–40, 1992.

[4] S. M. Kay. *Fundamentals of Statistical Signal Processing, Volume 2: Detection Theory*. Prentice Hall PTR, 1998.

[5] U. Mueller, M. Dacorogna, and O. Pictet. Hill, bootstrap and jackknife estimators for heavy tails. *In R. Adler, R. Feldman, and M. Taqqu (eds.), A Practical Guide to Heavy Tails: Statistical Techniques for Analysing Heavy Tailed Distributions*, pages 283–310, 1998.

[6] B. Silverman. *Density Estimation for Statistics and Data Analysis*. Chapman & Hall, 1986.